

Potential Impact of Interfacial Bonding Efficiency on Used Nuclear Fuel Vibration Integrity during Normal Transportation – 14502

Hao Jiang, Jy-An Wang, Hong Wang
Oak Ridge National Laboratory

ABSTRACT

The potential impacts of interfacial bonding efficiency at pellet–pellet and pellet–clad interfaces on surrogate of used nuclear fuel (UNF) was investigated using Finite Element Analysis (FEA) for its vibration integrity. Bending moments (M) are applied to the FEA models to evaluate the system responses of the surrogate rods. From the induced curvature, κ , the flexural rigidity EI can be estimated as $EI = M/\kappa$. The result indicates that the flexural rigidity of the surrogate rod and the bending moment bearing capacity between the clad and fuel pellets are strongly dependent on the efficiency of interfacial bonding at the pellet–pellet and pellet–clad interfaces. The FEA simulation results were also validated and benchmarked with reversible bending fatigue test results on surrogate rods consisting of stainless steel (SS) tubes with alumina-pellet inserts. FEA models will be further used to study UNF vibration integrity.

INTRODUCTION

It is important to understand the potential effect of varying degrees of bonding at the pellet–pellet and pellet–clad interfaces of the UNF system under normal transportation conditions including normal handling drops and transient shocks. FEA methods have been used to develop simulation protocols, in addition to experimental calibration and verification efforts, to investigate these effects.

This paper describes the methodology used to evaluate the potential effect of pellet–pellet and pellet–clad interactions with consideration of the interfacial bonding efficiency on UNF vibration integrity. This methodology has potential to provide a solid roadmap for further protocol development with respect to effective lifetime prediction of a UNF system under normal transportation vibration. The proposed methodology that couples FEA simulations and experimental exploration efforts is also under development. The current methodology is focused on assessing the influence of interfacial bonding at the pellet–pellet and the pellet–clad interfaces on UNF vibration integrity. The FEA simulation results were also calibrated and benchmarked with the fatigue aging data [2, 3] obtained from reversible bending fatigue testing of surrogate materials.

The objective of this paper is to investigate the potential impact of interfacial bonding efficiency at pellet–pellet and pellet–clad interfaces on surrogate of UNF for its vibration integrity. The FEA models, with a 50.8 mm gauge section that covered the SS clad and alumina pellets and with epoxy layers supplying cohesion, were developed with the ABAQUS code. In order to estimate the surrogate rod system responses including the stress profile and the associated curvature, κ , the bending moments (M) were applied to both ends of the surrogate rod. From the FEA results, the flexural rigidity (EI) of the simulation cases is estimated as $EI = M/\kappa$. Detailed discussions and comparisons of the simulation cases are organized as follows.

1. The section model with good interfacial bonding and without pellet fracture
2. The section model with good bonding at pellet–clad interfaces and de-bonding at pellet–pellet interfaces
3. The section model with de-bonding both at pellet–clad and pellet–pellet interfaces

The simulation results indicate that the system response and the associated flexural rigidity are strongly dependent on the interfacial bonding efficiency. The FEA simulation results are validated and calibrated by use of reversible bending fatigue testing on the surrogate SS rod with alumina-pellet inserts.

ANALYSIS OF INTERFACIAL BONDING EFFICIENCY OF SURROGATE RODS

Structural analysis and an interfacial bonding evaluation of the surrogate rods used in the bending fatigue testing system [2–4] were performed with the ABAQUS code. The reversible bending fatigue testing system used surrogate rods to calibrate and improve the test setup in an out-of-cell environment. To validate simulation results with out-of-cell surrogate data, the surrogate rod materials used in FEA are the same as those used in the out-of-cell testing. High-density alumina was selected as the pellet material, and SS 304 was used as the clad material. Epoxy was used as the interfacial bonding material. Material properties of the surrogate rod are listed in Table 1.

Table 1. Material properties of surrogate rod

Material	Young’s Modulus (GPa)	Poisson’s Ratio	Yield Strength (MPa)	Density (kg/m ³)
Stainless Steel ^a	193	0.300	290	8030
Al ₂ O ₃ ^{b,c}	372	0.220	2500	3920
Epoxy ^{d,e}	3.5	0.370	69	1251

^aProduct Data Bulletin, 304/304L stainless steel, AK Steel Corporation, <http://www.aksteel.com>

^bCeramic Properties Standard, CoorsTek, Inc., <http://www.coorstek.com>

^cThe mean flexural strength of the Al₂O₃ is around 48 ksi from the vendor McMaster-Carr.

^dMore about Glass, Ceramics, Carbon; More About Stainless Steel Alloys, Mechanical and Physical Properties, <http://www.mcmaster.com>

^ehttp://www.engineeringtoolbox.com/material-properties-t_24.html

Rods with Good Interfacial Bonding

Fig. 1 shows the geometry of a U-frame bending fatigue testing system with a co-planar configuration for the surrogate rod. The 50.8mm gauge section is highlighted in black. A finite element model was established to represent the 50.8mm gauge section of the test specimen, referred to as the Clad-Epoxy-Pellet section model. The inside and outside diameters (ID and OD) of the clad are 9.703 and 11.074 mm, respectively. The alumina

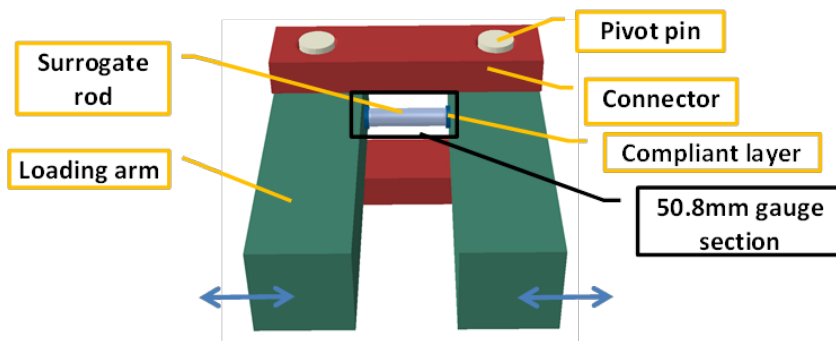


Fig. 1. Geometry of horizontal U-frame bending fatigue testing system with co-planar configuration of the rod.

pellet OD is 9.449 mm. The 50.8 mm gauge section of the surrogate rod contains two 15.24 mm pellets in the middle and two 10.16 mm pellets at the ends. The gap between the clad and the pellet was sized 0.127 mm and filled with a cast epoxy layer. The extent of epoxy filling and bonding apparently depends on the casting and the subsequent loading. However, the relevant

data were not available. In our modeling study, three conditions will be studied: 1) pellet–clad and pellet–pellet interfaces are bonded, 2) pellet–clad interfaces are bonded and pellet–pellet interfaces are de-bonded, and 3) pellet–clad and pellet–pellet interfaces are both de-bonded.

Bending moments were applied on both ends of the surrogate rod rotating along the x-axis. According to the out-of-cell surrogate data, the bending moments ranged from 20 to 30 N·m; the bending moment M_x was selected as 25 N·m. Both loading surfaces of the surrogate rod were constrained with rotation along y- and z-axes and translation along the x direction. In the following finite element models, the global mesh is 0.508 mm. Some local meshes are as small as 0.0635 mm. The quasi-static procedure used in FEA is from the ABAQUS code. The original surrogate rod was, in fact, 6 in. long with 10 alumina pellets [3–4]. The contact between neighboring pellets generally depends on the casting process. Gaps may exist between the pellets and may be filled with epoxy. Thin epoxy layers are tied to the gap surfaces at the pellet–clad interfaces and at the pellet–pellet interfaces to simulate cohesive bonding. The modeling study in the report considered the following aspects:

1. Gaps were filled with epoxy layers in which pellet–epoxy and epoxy–pellet interfaces were tied or bonded,
2. Gaps existed and were not filled with epoxy layers, and
3. No gap existed between neighboring pellets and pellet–pellet interfaces were de-bonded.

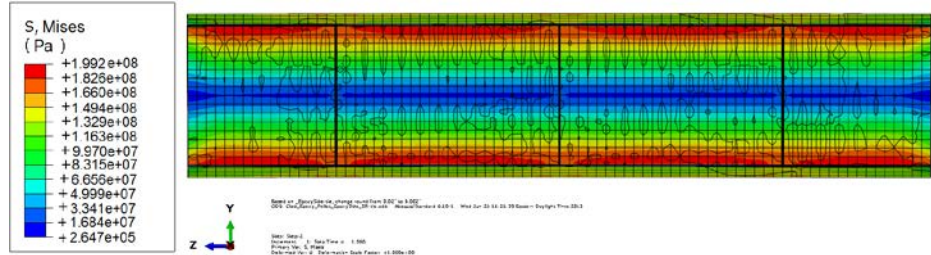
This model has three 0.0356 mm gaps filled with epoxy at the pellet–pellet interfaces. The resultant stress distribution and curvature are shown in Fig. 2. The resultant curvature is 0.157 m^{-1} , too small to be noticeable, as illustrated in Fig. 2(a). From the resultant stress distribution shown in Fig. 2, the maximum stress occurs at the outer surface of the alumina rod, and the resultant forces also indicate that the alumina pellets carry a larger portion of the moment resistance than the clad. The clad did not yield under a 25 N·m bending moment, nor did the alumina pellet, which has a much higher yield strength than the SS clad. This indicates that the surrogate rod in a perfectly bonded condition will remain within the linear elastic range under the target loading.

The curvature and flexure rigidity for this case is summarized in Table 2. In this case, a load control procedure was used, the bending moment M was applied to both ends of the surrogate rod, and the bending curvature κ was estimated from the FEA result within the gage section. Furthermore, the flexural rigidity EI (the product of Young's modulus E and moment of inertia I) of a surrogate rod can be estimated from the applied moment M and the resultant curvature κ .

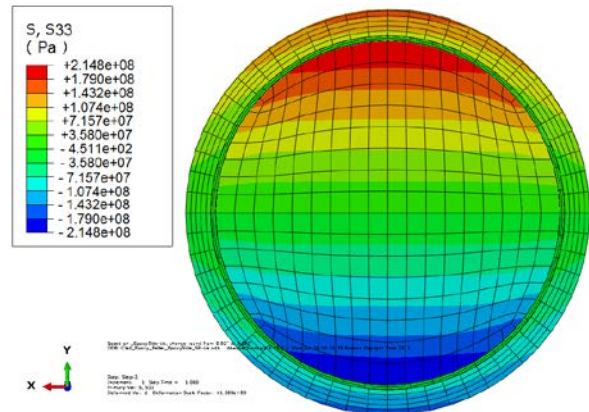
In surrogate rod SSAP05 [3], alumina pellets were bonded to the SS tube and to each other using epoxy. The SSAP05 specimen was tested up to the 25 N·m bending moment. High flexural rigidity was observed. The initial (first cycle) test data, which has the highest flexural rigidity on the left side, indicates that the bonds at the pellet–clad and pellet–pellet interfaces should remain intact at the corresponding curvature level. The flexural rigidity of the first test data is very close to the FEA estimation of $153 \text{ N}\cdot\text{m}^2$.

With good interfacial bonding, the alumina rod can carry most of the bending moment under normal transportation vibration because the Young's modulus of the alumina rod is twice that of the clad (Table 1). Due to the high yield strength of the alumina pellets, the surrogate rod can work within the linear elastic range to a large extent. The high flexural rigidity estimated from FEA (Table 2) is in good agreement with that estimated from bending fatigue testing data. Thus, the epoxy layers fully bonded to the surfaces of gaps in both clad–pellet and pellet–pellet directions

would capture the earlier elastic behavior of the surrogate rod, and the structural integrity of interfaces should be maintained.



(a) Longitudinal cut view of resultant curvature and von Mises stress



(b) Cross-sectional view of resultant σ_{zz} at a pellet–pellet interface

Fig. 2. Normal stress distribution and curvature resulting from Clad-Epoxy-Pellet section model with four pellets and epoxy-filled gaps at pellet–pellet interfaces.

Table 2. Curvature and flexural rigidity for the perfect interfacial bonding simulation

Designation	Curvature, κ (1/m)	Bending moment, M (N·m)	Flexural rigidity, EI (N·m ²)	Note
Clad-Epoxy-Pellet4-Tie-Pellet-Epoxy-Tie-at Gap	0.163	25	153	Gaps between neighboring pellets filled with epoxy; pellet–epoxy and epoxy–pellet interfaces bonded

Symmetrical reversible output force was obtained for the composite rod (SS tube + alumina rod) using an U-frame bending fatigue testing system. Displacement control was used for bending tests with amplitudes of 3 to 13 mm with a frequency of 0.1 Hz, and the deflection was measured at the midpoint of the rod. The composite rod bending test results indicate that before the inserted alumina rod fracture, the composite rod responded linearly and most of the bending load carrying capacity resided on the alumina rod due to a Young’s modulus that was twice that of the SS clad. Upon the alumina insert fracture, sudden load transfer occurred and the SS tube started to carry the majority of the bending moment, which resulted in plastic deformation of SS clad, as will be demonstrated in the following simulation cases.

Effect of Pellet–Pellet Interfacial Bonding Efficiency

Before being transported, the UNF system may exhibit inherited stress fields, such as axial tensile stress and tangential tensile stress due to pellet–clad mechanical interaction, or due to oxide volume expansion, as well as radial compressive stress due to hydride compaction and tangential shear stress due to hydride volume expansion. Vibration during transportation will result in bending loads on the UNF assembly. If the loads are significant enough to induce repeated expansion and contraction in both the axial and tangential directions of the UNF rod due to reversible bending flexural deformation, combined with stress concentration, has potential to degrade the interfacial bonding at fuel pellet–clad interfaces and pellet–pellet interfaces, as shown in Fig. 3. While the shear stress is small relative to the normal stress due to bending, it does not mean that it can be neglected. In particular, in a composite rod or UNF rods, excessive shear due to material mismatch can be a cause of failure for interfacial bonding.

At pellet–pellet interfaces, interfacial bonding fails mainly from normal stress due to reversible bending flexural deformation, combined with relatively less shear stress, as shown in Fig. 3; at pellet–clad interfaces, localized high shear stress will also arise to compensate for the material mismatch under flexural deformation. As mentioned above, the shear stress is small relative to the normal stress; thus, it is likely that the interfacial bonding failure at pellet–pellet interfaces will occur before the de-bonding at pellet–clad interfaces. Observation of the ORNL reversible bending fatigue of the surrogate SS rod with alumina pellets verified this hypothesis. In this section, the Clad-Epoxy-Pellet section model with four pellets was used to investigate the surrogate rod bending response with perfect bonding at pellet–clad interfaces, but various de-bonded states at pellet–pellet interfaces were the focus. The material properties, geometry, and loading and boundary conditions are the same as those used in the previous FEA simulation.

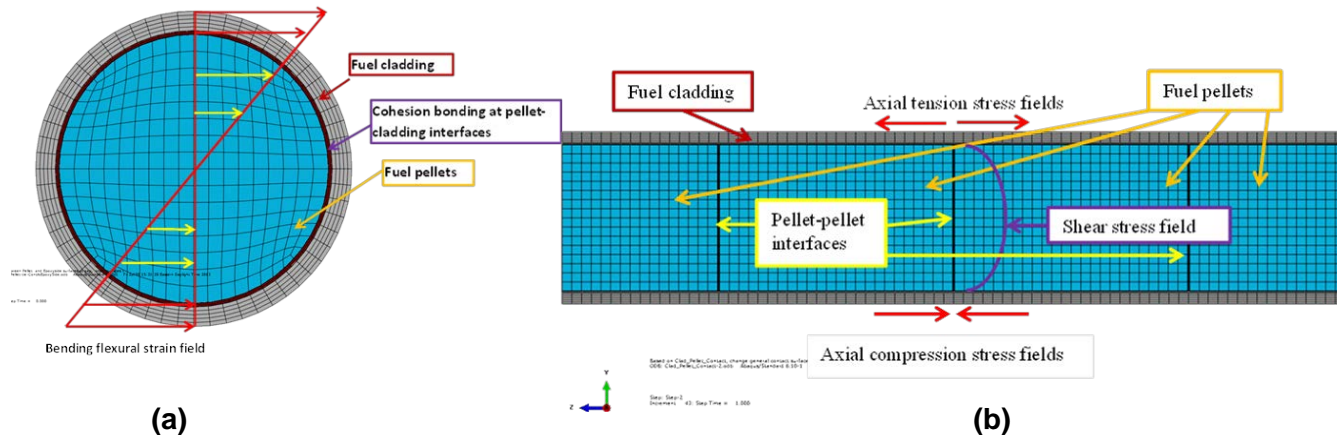


Fig. 3. Transportation-induced reversible bending stress fields in a UNF system.

The first case study of pellet–pellet interfacial de-bonding was dedicated to gaps at pellet–pellet interfaces without epoxy, while a thin epoxy layer still existed at pellet–clad interfaces and was tied to the adjacent surfaces to provide perfect cohesion.

Compared to the results shown in Fig. 2, there are significant differences in the stress distribution between the case of pellet–pellet interfacial bonding and the case of pellet–pellet interfacial de-bonding, where perfect bonding remains for both pellet–clad interface cases. For instance, for the pellet–pellet interface of the de-bonded case, the maximum tensile stress, which reaches the yield strength of clad at 289.6 MPa, occurs at the clad and is located at both the top and bottom

sides near the pellet–pellet interface regions. The curvature profile shows a lateral contraction and lateral expansion at the compression and tension sides of the clad, respectively. Particularly, a localized clad buckle developed near the pellet–pellet gaps, likely due to the lack of internal support. On the compression side, the clad deforms continuously when the pellet–pellet surfaces are being driven together until the gaps are closed. No stress concentrations are observed at pellet–pellet contact corners. Resultant σ_{zz} clearly indicates that the intensely stressed clad takes over more bending moment resistance than that of the pellets at the de-bonded pellet–pellet interfaces.

At the de-bonded pellet–pellet interfaces, the pellets can only transfer load via hard contact, so the load carrying capacity shifts significantly from pellets to the clad. The SS tube starts to carry the majority of bending moment at the tension-side near the pellet–pellet interface region, which results in a significant localized plastic deformation at the SS clad. Over most of the gauge section, the pellets still provide sufficient internal support to the clad due to good cohesion at the pellet–clad interfaces and will carry most of the bending load; therefore, there is no yielding at most regions of the SS clad. The results are contrary to the results of the perfectly bonded case in Fig. 2, which shows that the pellets carry significant bending moment resistance; the maximum stress resides at the pellets, and there is no yielding at either the pellets or the clad.

It is also interesting to note that the von Mises stress distribution in the de-bonded pellets case appears to be in a dog-bone shape due to contact pressure at pellet–pellet interfaces. This also differs from the results of the bonded pellet–pellet interface case. The third discrepancy lies in the induced curvature. In the de-bonded case, the resultant curvature is 0.669 m^{-1} , which is four times that of the perfectly bonded case shown in Fig. 2.

The second case on the de-bonded pellet–pellet interface is no gap at pellet–pellet interfaces before applying a bending load. As in previous cases, a thin epoxy layer is applied and tied to surfaces at pellet–clad interfaces to simulate good cohesive bonding.

The stress distribution of this case appears to be similar to that with gaps between the de-bonded pellet–pellet interfaces. The SS clad also yields at the top tensile side near the pellet–pellet interface regions; however, on the compression side, the maximum stress occurs at the pellets instead of clad. Nevertheless, the pellet is within the linear elastic range overall due to its high yield strength. From the curvature profile, no clad buckling is observed at the bottom (compression) region. This is because of the absence of gaps at the pellet–pellet interface region; thus, the compacted pellets provide good internal support to the clad tubing structure. Furthermore, pellets seem to carry a significant portion of bending moment resistance via pellet–pellet interaction (pinching at pellet corners), which significantly mitigates the stress level of the clad at the bottom (compression) region.

The pellet stress profiles also show a dog-bone shape due to contact pressure at the pellet–pellet interfaces. The resultant σ_{zz} profile with no gaps at the pellet–pellet interface indicates that these pellets can carry more bending moment resistance than pellets with gaps. The induced curvature of this pellet–pellet interface de-bonding with gaps case is 0.241 m^{-1} , much smaller than that of previous cases.

Table 3 summarizes the estimated curvature and the flexural rigidity based on the two pellet–pellet interface cases discussed in this section. The comparison between results in Tables 2 and 3 suggests that the immediate consequence of the de-bonded pellet–pellet interface is a significant increase in curvature, and this, in turn, results in a significant reduction in the estimated

flexural rigidity. This phenomenon is primarily due to the load carrying capacity shifting from the pellets to the clad.

Table 3. Curvature and flexural rigidity for the bonded pellet–clad and de-bonded pellet–pellet cases

Designation	Curvature, κ (1/m)	Bending moment, M (N·m)	Flexural rigidity, EI (N·m ²)	Note
Clad-Epoxy-Pellet4-Tie-Pellet-Contact-Gap	0.669	25	37	Gaps between neighboring pellets had no epoxy filling
Clad-Epoxy-Pellet4-Tie-Pellet-Contact-No Gap	0.241	25	104	No gap between neighboring pellets; pellet–pellet interfaces were de-bonded

Table 3 shows that the gaps at pellet–pellet interfaces play a critical role in estimating the flexural rigidity of the surrogate rod. The induced curvature of 0.669 m⁻¹ for the case of gaps is four times that of the perfectly bonded interface case. The curvature increase corresponds to a 76% reduction in flexural rigidity, from 153 N·m² for the perfectly bonded interface case to 37 N·m² for the case of empty gaps. When the gaps are eliminated, the flexural rigidity value can go as high as 104 N·m². The above indicates that the gap-induced large plastic deformations of SS clad at the pellet–pellet interface region can lead to significant reduction in the bending stiffness, or, the flexural rigidity (EI) of the surrogate rod system. If there are no gaps at the pellet–pellet interfaces, the pellets can carry a significant portion of bending moment resistance via direct pellet–pellet contact (interaction) to mitigate the potential yield of the clad.

Effect of Gaps between Pellets with De-Bonded Pellet–Clad Interfaces

Under a flexural deformation, high shear stress will arise at pellet–clad interfaces to compensate for the material mismatch, in addition to the flexural shear stress in the UNF system. Thus, under a reversible bending load during normal transportation, both cyclic normal stress and shear stress may further degrade the interfacial bonding at fuel pellet–clad interfaces. In this section, de-bonded pellet–clad interfaces and de-bonded pellet–pellet interfaces cases are investigated using a Clad-Epoxy-Pellet section model with four pellets. The surrogate rod consisting of SS clad and alumina pellet inserts is used to study the system response to bending moment with de-bonded interfaces. Loading and boundary conditions are the same as those of the previous cases, and the assigned bending moment is 25 N·m. The first simulation case of interfacial de-bonding is at both pellet–clad and pellet–pellet interfaces. There are empty gaps at the de-bonded pellet–pellet interfaces and a thin epoxy layer at the de-bonded pellet–clad interfaces.

The resultant stress distribution indicates that the yielded SS clad almost extends throughout the whole gauge section, when the interfacial de-bonding occurs at both pellet–clad and pellet–pellet interfaces. This is in great contrast to the results in only pellet–pellet de-bonding cases, where the SS tube only locally yields at pellet–pellet interface regions and the maximum stress resides at pellets on the compression side of pellet–pellet interfaces. The pellets were all below yield at the maximum stress level due to high yield strength. The pellet stress contours also show a dog-bone shape due to pellet–pellet contact interaction. The induced curvature of 0.727 m⁻¹ is large enough to be visualized from the longitudinal cut view without increasing the scale. It suggests that due to

the interfacial de-bonding both at pellet–clad and pellet–pellet interfaces, the contained pellet inserts and the SS clad can only make contact at the pellet–pellet and pellet–clad interface regions, and the pellets cannot provide direct internal support to the clad. Therefore, the load shifts significantly from pellets to the clad over the entire gauge section; the results also indicate that the SS clad carries the majority of the bending moment. The bending deformations in the de-bonded pellet–clad region will likely result in further pinching action at pellet–clad interfaces, which may also result in an accelerated aging of the clad tubing.

The second case in this section is where a thin epoxy layer is filled at de-bonded pellet–clad interfaces and the pellets are all in direct contact with each other with no gaps at the pellet–pellet interfaces. The loading and boundary conditions as well as material properties are the same as those of the previous cases. The surrogate rod responses to the bending moment upon interfacial de-bonding without gaps at the pellet–pellet interfaces shows that the SS clad yields at the top (tension) region throughout the gauge section but remains elastic at the bottom (compression) region. The maximum stress still occurs on the compression side of the pellet region where the pellets are pinching each other. The interfacial results are similar to those observed for the bonded pellet–clad interfaces and de-bonded pellet–pellet interfaces without gaps. The pellets carry a large portion of the bending moment resistance via pinching pellet corners and reduce the stress intensity of the bottom (compression) portion of the clad. The major difference from the results is the extensive plastic deformations observed at the top region of the SS tube throughout the entire gauge section, instead of the localized yielding observed at the interface region in the case of only pellet–pellet interfacial de-bond. Due to the lack of a direct load transferring mechanism from pellet to clad or vice versa because of de-bonded pellet–clad interfaces, the clad takes over the majority of the bending moment resistance.

The results of the evaluated curvature and flexural rigidity for the cases of de-bonding at pellet–clad and pellet–pellet interfaces are listed in Table 4. Compared to the results of the de-bonded pellet–pellet interface case listed in Table 3, the flexural rigidities are further decreased by 8% (from 37 N·m² to 34 N·m²) for pellets with gap cases and by 19% (from 104 N·m² to 84 N·m²) for pellets with no gap cases. This result further validates the earlier hypothesis in the case of pellet–clad interfaces, that interfacial bonding efficiency can significantly affect the flexural rigidity of the surrogate composite rod.

Table 4. Curvature and flexural rigidity for de-bonded pellet–clad and pellet–pellet interfaces

Designation	Curvature, κ (1/m)	Bending moment, M (N·m)	Flexural rigidity, EI (N·m ²)	Note
Clad-Epox-Pellet4- Contact-Pellet- Contact-Gap	0.727	25	34	Gaps between neighboring pellets had no epoxy filling
Clad-Epoxy-Pellet4- Contact-Pellet- Contact-No Gap	0.298	25	84	No gap between neighboring pellets; pellet–pellet interfaces were de-bonded

In Table 4, the flexural rigidity of the case with no gaps at pellet–pellet interfaces is 2.5 times that of the case with gaps. In Table 3, the same comparison of flexural rigidity results in a similar ratio of 2.8. The reason for the large increase in flexural rigidity is the direct contact of the pellets at the

pellet–pellet interfaces on the compression side. The direct pellet–pellet contact provides a significant increase in bending moment resistance, resulting in much less curvature deformation, as shown in Table 4.

CONCLUSION

Based on the FEA simulation results and further verification from ORNL surrogate rod bending test results, the impacts of interfacial bonding efficiency at pellet–pellet and pellet–clad interfaces on surrogate rod system performance can be summarized as follows.

First, with good interfacial bonding and without surrogated fuel pellet and clad fracture, the pellets in the surrogate rod will carry more bending moment resistance than the clad under normal transportation vibration. The maximum stress resides at the pellets, and the stresses at the clad and pellet are both below the yield condition; therefore, the system is in a linear elastic state under the target bending loads.

Upon surrogated fuel pellet failure including de-bonding at the pellet–pellet interfaces, the load carrying capacity shifts from fuel pellets to the clad, and the clad starts to carry the majority of the bending moment at the pellet–pellet interface region, which results in localized plastic deformation of the clad. With good cohesion at the pellet–clad interfaces, the pellets can still provide support to the clad and carry a sufficient portion of the bending moment resistance, so that a major portion of the clad at the gauge section remains in the linear elastic range.

Upon further de-bonding at the pellet–clad interfaces, the embedded pellets can no longer provide effective structural support to the clad as well as assist the load transfer within the surrogate rod system. Thus, the majority of the load carrying capacity shifts to the clad throughout the entire gauge section. That leads to the clad yielding in the entire gauge section instead of at localized pellet–pellet interface regions. When the pellets contact and pinch each other, the pellets seem to take over a significant portion of the bending load resistance, especially for cases where there are no gaps at the pellet–pellet interfaces. This pellet pinning action certainly mitigates and avoids the clad yielding, and the maximum stress resides at the pellet region and below the yield.

Table 5. Comparison of flexural rigidity between different bonding and de-bonding cases

	Flexural rigidity, EI (N·m ²)	Reduction from perfect bonding (%)	Increase from with gaps to without gaps (%)
Perfectly bonded	153		
De-bonded pellet–pellet interfaces with gaps	37	76	
De-bonded pellet–pellet and pellet–clad interfaces with gaps	34	78	
De-bonded pellet–pellet interfaces without gaps	104	32	64
De-bonded pellet–pellet and pellet–clad interfaces without gaps	84	45	60

The immediate consequence of interfacial de-bonding is the load carrying capacity shift from surrogate fuel pellet to clad, as well as the reduction of flexural rigidity, as shown in Table 5. Compared to the flexural rigidity of 153 N·m² for a perfect bond, the flexural rigidity for the de-bonding at pellet–pellet interfaces alone is reduced by 76% (to 37 N·m²) in the case with gaps at the pellet–pellet interfaces and by 32% (to 104 N·m²) for the case with no gaps. Upon further de-bonding at the pellet–clad interfaces, the flexural rigidity is further reduced by 8% and 19% for the cases with gaps and without gaps, respectively. The overall reductions from the perfectly bonded case to the de-bonded case at all interfaces are about 78% and 45%, respectively, for the cases with gaps and without gaps.

More reductions in flexural rigidity are due to de-bonding at pellet–pellet interfaces than due to de-bonding at pellet–clad interfaces. Table 5 shows about a 60% increase in the flexural rigidity from the case with gaps to the case without gaps, which indicates a significant increase in system stiffness for the surrogate rod without gaps. Therefore, gaps at the interfaces of the surrogate rod system can have a significant impact on system reliability, especially at pellet–pellet interfaces.

The flexural rigidity and bending moment resistance capacity of the surrogate rod system are strongly dependent on the efficiency of interfacial bonding at pellet–clad and pellet–pellet interfaces. This discovery was also validated by integrated cyclic reversible bending fatigue test (CIRFT) results performed on the surrogate SS rod with alumina pellets inserts. Its application to the UNF is still pending on further verification from UNF CIRFT test results. The surrogate rod system was designed to resemble the UNF system, and the results provide theoretical insight on the complexities of the UNF system. However, a direct and correlated relationship between the surrogate rod system and irradiated material has not yet been established.

REFERENCES

1. US Department of Energy, Used Fuel Disposition Campaign, *Used Nuclear Fuel Loading and Structural Performance under Normal Conditions of Transport – Modeling, Simulation and Experimental Integration RD&D Plan*, FCRD-UFD-2013-000135, April 1, 2013.
2. J.-A.J. Wang, H. Wang, Y. Yan, R. Howard, B. Bevard, *High Burn-up Spent Fuel Vibration Integrity Study Progress Letter Report (Out-of-Cell Fatigue Testing Development – Task 2.1)*, ORNL/TM-2010/288, Oak Ridge National Laboratory, Oak Ridge, TN, 2011.
3. J.-A.J. Wang, H. Wang, T. Tan, H. Jiang, T. Cox, Y. Yan, *Progress Letter Report on U-frame Test Setup and Bending Fatigue Test for Vibration Integrity Study (Out-of-Cell Fatigue Testing Development – Task 2.2)*, ORNL/TM-2011/531, Oak Ridge National Laboratory, Oak Ridge, TN, 2012
4. H. Wang, J.-A.J. Wang, T. Tan, H. Jiang, T. Cox, R. Howard, B. Bevard, M. Flanagan, “Development of U-Frame Bending System for Studying the Vibration Integrity of Spent Nuclear Fuel,” *Journal of Nuclear Material* **440**, 201–213, 2013.

ACKNOWLEDGEMENTS

This research was sponsored by DOE UFDC and was conducted at Oak Ridge National Laboratory under contract DE-AC05-00OR22725 with UT-Battelle, LLC. The authors would like to thank Program Managers Harold Adkins, Bruce Bevard, and Rob Howard for providing guidance and support to this project.